DOI: 10.1002/((please add manuscript number))
Article type: Communication

Superior performance of Silver Bismuth Iodide photovoltaics fabricated via dynamic hot-casting method under ambient conditions

*Biplab Ghosh, Bo Wu, Xintong Guo, Padinhare C. Harikesh, Rohit Abraham John, Tom Baikie, Arramel, Andrew T. S. Wee, Claude Guet, Tze Chien Sum, Subodh Mhaisalkar, and Nripan Mathews**

Biplab Ghosh, P. C. Harikesh, Dr. Tom Baikie, Prof. Claude Guet, Prof. Nripan Mathews, Prof. Subodh Mhaisalkar
Energy Research Institute @ Nanyang Technological University (ERI@N)
50, Nanyang Drive
Singapore 637553

Biplab Ghosh, X. Guo, P.C. Harikesh
Interdisciplinary Graduate School
Nanyang Technological University
Singapore 639798

Dr. Bo Wu, Prof. T. C. Sum
Division of Physics and Applied Physics, School of Physical and Mathematical Sciences
21 Nanyang Link
Nanyang Technological University
Singapore 637371

Dr. Arramel, Prof. A. T. S. Wee
Department of Physics
National University of Singapore
2 Science Drive 3
Singapore 117542

R. A. John, Prof. C. Guet, Prof. S. Mhaisalkar, Prof. N. Mathews
School of Materials Science and Engineering
50 Nanyang Avenue
Nanyang Technological University
Singapore 639977
E-mail: nripan@ntu.edu.sg

Keywords: perovskite solar cells, lead-free perovskites, Bi-based ternary halides, dynamic hot casting

Abstract: Bismuth-based ternary halides have recently gained a lot of attention as lead-free perovskite materials. However, photovoltaic performances of these devices remained poor, mostly due to their low dimensional crystal structure and large bandgap. Here we demonstrated

a dynamic hot casting technique to fabricate silver bismuth iodide-based perovskite solar cells under ambient atmosphere with power conversion efficiencies above 2.5%. Silver bismuth iodides are 3-dimensional analogs of complex ternary bismuth halides with a suitable bandgap for a single junction solar cell. To the best of our knowledge, these results represent the highest efficiency for solution processed air-stable lead-free perovskite solar cells. The enhanced solar cell performances via dynamic hot casting technique can be attributed to long carrier lifetimes, micron-sized crystalline grains, and pinhole free thin-film formation with uniform morphology. This work provides a new direction for fabrication of solution-processed lead-free perovskite solar cells with a rapid fabrication strategy irrespective of the processing environment.

Solution-processed lead halide perovskites have established themselves as one of the most important absorber materials in solar cells with power conversion efficiencies now exceeding 22%.[1] Unfortunately, the over reliance on highly toxic Pb^{2+} remains a key issue for widespread commercial applications. The significant concentration of Pb^{2+} in high performing halide perovskites and its water solubility make it highly hazardous compound to the environment.[2] Another apparent issue is the inherent instability of lead-based halide perovskites in ambient atmosphere.[3] Although the stability of Pb-based halide perovskites has improved impressively in recent times along with the simultaneous development of passivation techniques, the fabrication of lead-based halide perovskites still requires stringent environmental control.[4] To address these potential issues, there is an increased interest towards lead-free halide perovskites and their analogues in photovoltaics. Replacing Pb^{2+} with Sn^{2+} or Ge^{2+} could minimize the toxicity associated with lead-based halide perovskite, however, the increased environmental instability of these compounds poses significant challenges in solar cell development.[5] Even after incorporating 2D/3D mixtures of perovskites, the efficiency of the highest performing Sn-

based system reduced to nearly 50% of its original value within 3 days under 20% humidity.[6] Considering atmospheric stability, trivalent cations such as bismuth and antimony-based ternary halides were also investigated as potential absorber materials due to their inherent atmospheric stability and low toxicity.[7] The incorporation of protonated cations such as MA or Cs with Bi-I octahedra forms Bi-based ternary halides (structural formula $A_3Bi_2I_9$: A = Cs, MA) that exhibit high absorption coefficients and facile solution processability. Nevertheless, the photovoltaic performances of Bi-based ternary halides remained poor mostly due to high optical bandgap and low electronic dimensionality.[8] Replacement of the A-site protonated cations with transition metals such as Ag or Cu is a promising strategy to improve the dimensionality. These transition metals also take part in bonding with Bi-I octahedra, resulting in complex halide bismuthates. In comparison to ternary bismuth iodides, silver/copper bismuth iodides offer a 3-dimensional edge-sharing octahedral network along with reduction of optical bandgap, which is an added advantage for photovoltaics. The iodobismuthates have been studied for several decades due to their interesting optoelectronic properties and super ionic conductivity.[9] Nonetheless, the photovoltaic applications of these compounds were not realized until Sargent and coworkers reported 1.22% power conversion efficiency with $AgBi_2I_7$ as the absorber material.[10] Later, *Zhu et.al.* achieved a 2.1% power conversion efficiencies with hexagonal Ag_2BiI_5 phase in as mesoscopic solar cell architecture, fabricated under an inert atmosphere.[11] Recently, *Turkevych et. al.* reported a maximum efficiency of 4.3% with Ag_3BiI_6 as the absorber material.[12] However, fabrication of these silver bismuth iodide phases involved solid state reaction above 500 ℃, followed by dissolution and spin coating on mesoporous TiO_2. Here, we present a dynamic hot casting (DHC) method to achieve high PCE of 2.2% with $AgBiI_4$ and 2.62% with Ag_2BiI_5 respectively, as photovoltaic absorbers in a mesoscopic architecture. Compared to the previous studies, the solar cells were fabricated under an ambient atmosphere (average RH ≥ 65%) via a single step spin coating technique without any need for antisolvent treatment. Details of the DHC technique are elaborated in the materials

and methods section. In short, hot precursor solutions were drop casted onto preheated substrates during the spinning stage (**Figure 1(a)**). This resulted in thin-films that exhibited pinhole free uniform morphology with large crystalline grains. In addition, DHC also enabled a better control over stoichiometry as AgI has a poor solubility at room temperature in commonly used organic solvents such as dimethylformamide (DMF) and dimethylsulphoxide (DMSO).

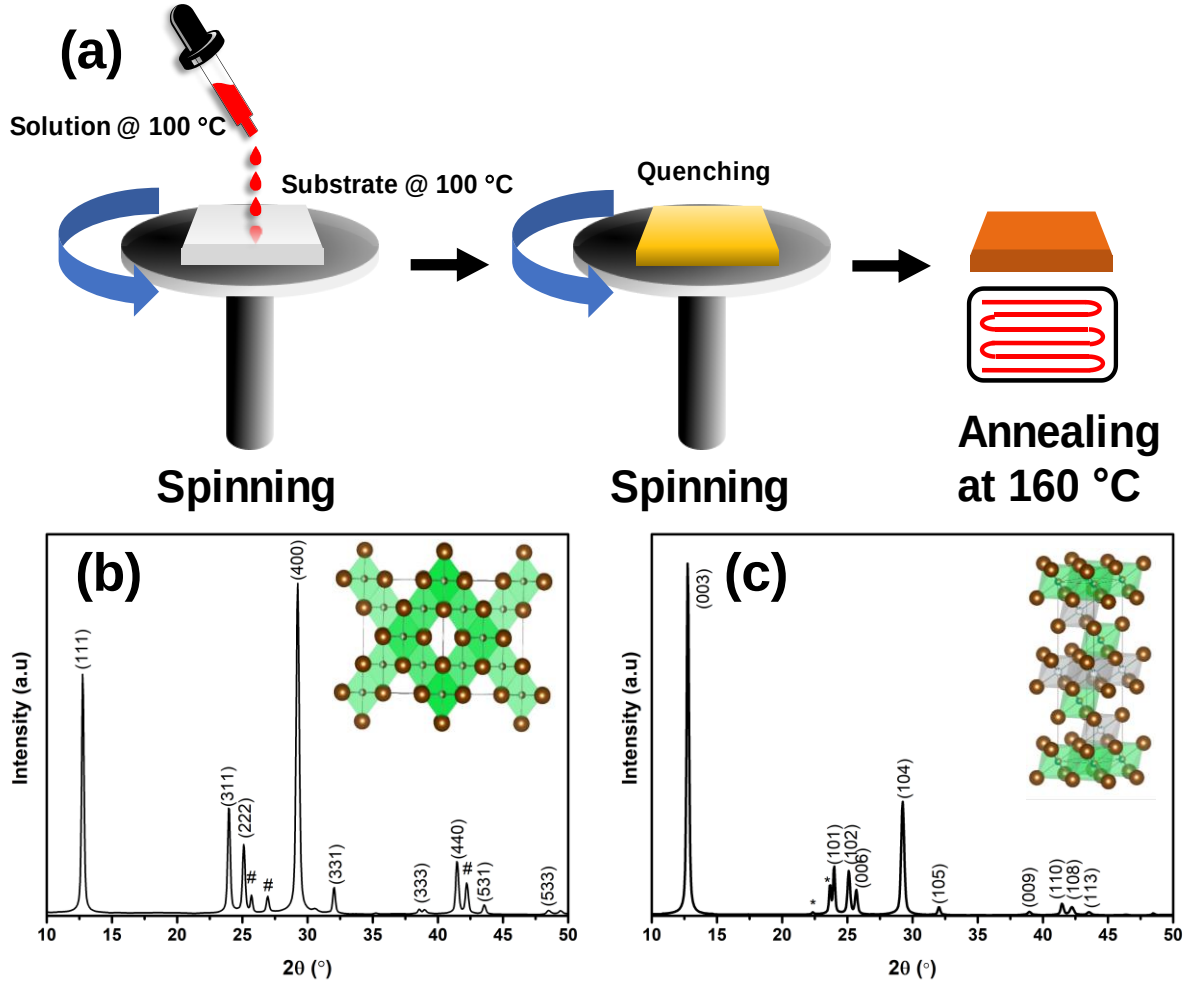

Figure 1: (a) Schematic illustration of dynamic hot casting technique, (b) powder XRD pattern of $AgBiI_4$ thin-films (inset: cubic structure of $AgBiI_4$), (c) powder XRD pattern of Ag_2BiI_5 phase (inset: crystal structure of hexagonal Ag_2BiI_5 phase)

Four different phases of Ag-Bi-I ternary system have been reported so far, namely, $AgBiI_4$, Ag_3BiI_6, Ag_2BiI_5 and $AgBi_2I_7$.[9, 13] Of these, $AgBi_2I_7$ was found to be energetically unfavorable.[14] The apparent phase with nominal composition $AgBi_2I_7$ was concluded to be an Ag-deficient $AgBiI_4$ (**Figure 1(b)(inset)**), otherwise it would lead to an unphysically short Bi-I bond length. On the other hand, both Ag_3BiI_6 and Ag_2BiI_5 possess a trigonal crystal structure ($R\bar{3}m$) with similar lattice constants (**Figure 1(c)(inset)**).[13] Recent work by *Jung et. al.* suggested that only Ag_2BiI_5 can be formed by solid-state reaction and is independent of precursor compositions.[15] Our observations are consistent with this, as the Ag_2BiI_5 phase was predominantly present in the thin-films fabricated via spin coating technique, even after varying compositions (Figure S1). With increasing Ag-to-Bi molar ratio, the reflections from unreacted AgI became increasingly evident in the X-ray diffraction (XRD) patterns. However, the use of a non-stoichiometric precursor solution resulted in crystallization of the Ag-deficient $AgBiI_4$ (Figure 1(b)). Presence of some impurity phases were noted in our observations (marked with # in Figure 1(b)), which can be assigned with either BiI_3 or Ag_2BiI_5 phase as the reflection positions are quite similar for Ag-deficient $AgBiI_4$, Ag_2BiI_5 and BiI_3. For high Ag-to-Bi molar ratios, the XRD analysis of the spin-coated thin-films revealed reflections consistent with the impurity phases AgI (marked with * in Figure 1(c)) and Ag_2BiI_5.

Figure 2 shows the surface morphology of normal spin coated (NSC) and dynamic hot casted (DHC) thin-films of $AgBiI_4$ and Ag_2BiI_5 phase by Scanning Electron Microscopy (SEM). As evident from the images, the thin-films fabricated via DHC method exhibited better surface coverage and uniform morphology with large crystallite size as compared to the thin-films fabricated by NSC. A plausible explanation for this observation is that the DHC method offers a better control over local supersaturation of the precursor solution. In typical spin coating, the morphology and crystallite sizes of the thin-films depend on the nucleation and grain growth, which again depends on the level of precursor supersaturation.[16] Now, for Pb-based halide perovskites, the most common way to control the level of supersaturation is the use of

antisolvents. In conventional antisolvent-assisted thin-film fabrication, the solubility of the precursor is high (high level of supersaturation necessary for nucleation) at the beginning of spin coating. During spinning, antisolvent is suddenly added on the film surface, which reduces the solubility of the precursor in the solvent (low level of supersaturation is sufficient for nucleation), resulting in rapid and uniform nucleation onset and therefore compact film morphology. The use of antisolvents to control the supersaturation during spinning has been successfully demonstrated in fabricating lead-based halide perovskite thin-films devices with superior performances.[17] However, a similar treatment on silver bismuth iodide resulted in voids and pinholes after thermal annealing (Figure S2). We speculate that due to fast crystallization process during antisolvent treatment, some of the DMSO remain entrapped inside the thin films (due to high boiling point of 189 ℃).[12] During the post-annealing process, the excess solvent creates voids inside the thin-films and resulted in poor morphology. We have also observed similar effects with conventional hot casting technique. On the other hand, in DHC, hot precursor solution was dripped slowly on the hot substrate during the spinning stage. We hypothesize that nucleation does not start at the initial contact with the mesoporous layer because of the high surface temperature. However, as the centrifugal force during spinning allowed the solvent to be removed simultaneously, it resulted in a supersaturated solution on top of the mesoporous TiO_2 layer. This resulted in a rapid nucleation onset with very little solvent to be left for trapping. As the dripping process is continuous, it allowed to have a layer-like precipitation on top of TiO_2 and subsequently grain growth takes place during post annealing process. Hence, unlike the commonly used antisolvent treatment in which the crystallization starts on the top of the films, the mesoporous TiO_2 surface acts as a nucleation site in DHC method, which resulted in uniform and compact thin-films.

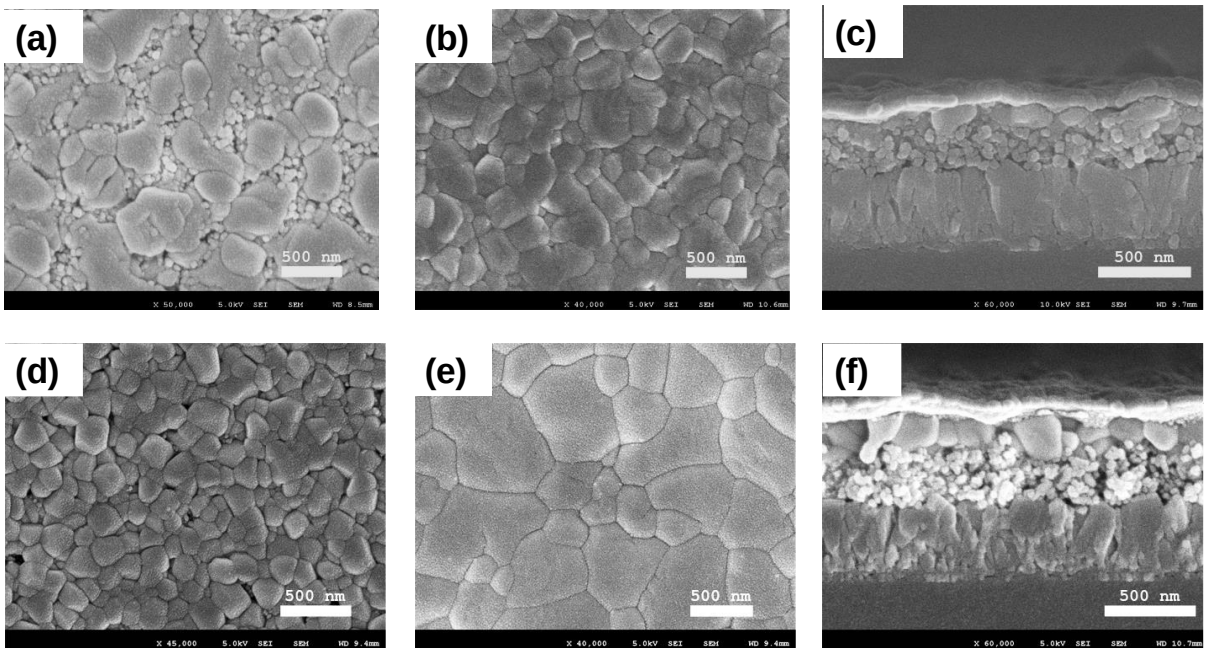

Figure 2: Scanning Electron Microscopy images of the normal spin coated (a), dynamic spin coated thin films of $AgBiI_4$ (b), normal spin coated (d) and dynamic spin coated thin films of Ag_2BiI_5(e), (c) and (f) illustrates the solar cell device cross-section of dynamic spin coated thin films of $AgBiI_4$ and Ag_2BiI_5 respectively.

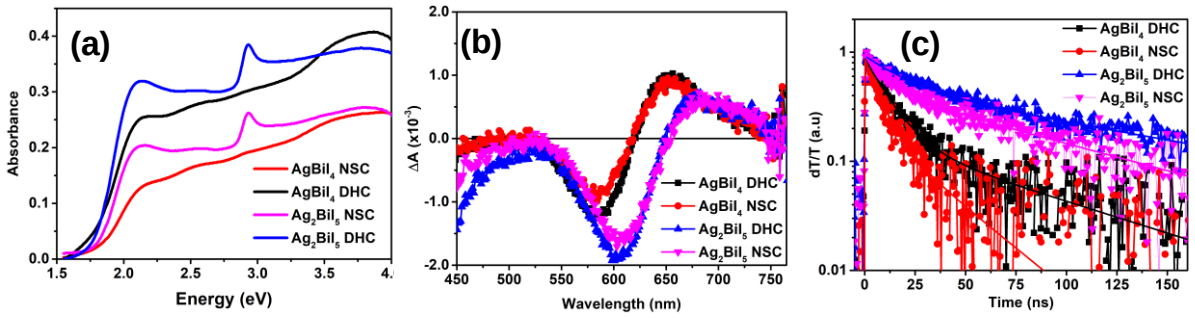

Figure 3: (a) UV-Vis absorption spectra, (b) Transient absorption spectra (at 1 ns), and (c) PB decay dynamics (at around 590 nm or 605 nm) silver bismuth iodide thin-films fabricated with different spin coating techniques

Figure 3(a) illustrates the absorption spectra of $AgBiI_4$ and Ag_2BiI_5 thin-films fabricated by NSC and DHC methods. Although the absorption onsets remained same for both methods, the thin-films fabricated by the DHC technique displays higher absorption than the NSC films for similar thickness, probably due to reduction of pinholes. The band gaps extracted from Tauc

plot for the indirect bandgap relationship gave 1.66 eV and 1.7 eV for $AgBiI_4$ and Ag_2BiI_5 respectively, which are in good agreement with previous reports.[11, 12, 15] The absorption spectrum of Ag_4BiI_7 showed a distinct absorption peak around 3 eV, which may be due to excess AgI in the thin-films as indicated by the XRD analysis. The compounds did not show any photoluminescence under the illumination of light, in accordance with indirect nature of the bandgap. Since radiative processes are not prevalent in this system, the excited-states carrier kinetics were monitored through transient absorption (TA) spectroscopy. As shown in **Figure 3(b)**, the kinetics of the excited state carriers are similar for both NSC and DHC thin-films for the phases. The TA spectra showed a strong photo-bleaching (PB) feature (i.e., negative ΔA) around 2.1 eV (~590 nm) and 2.05 eV (~605 nm) for $AgBiI_4$ and Ag_2BiI_5 respectively, followed by a photo-induced absorption (PIA) (i.e., positive ΔA) peak at longer wavelengths. Note the PB peak positions in both compounds do not correspond to their steady-state absorption edges, instead, they have the same position with the small hump near the absorption edges. This indicates the absorption edge of the two films comprise of an absorption continuum and an exciton absorption band which are not spectrally well resolved. The PB is then due to the change of the excitonic absorption resulting from the photoexcited carrier relaxation to the indirect band edge. Using Elliot's equation, we can extract the direct bandgap of the 2.37 eV and 2.2 eV for $AgBiI_4$ and Ag_2BiI_5 respectively. The direct exciton binding energies as determined by the fittings are around 260 meV and 150 meV for $AgBiI_4$ and Ag_2BiI_5 respectively (Figure S3). However, these numbers are only approximate due to the broadness of the spectra lines that arise from system disorder. Nevertheless, the fitting results can perfectly explain the observed TA profiles by involving exciton absorption. Carriers which relax to the indirect band edge can change the excited state exciton feature (oscillation strength, linewidth, and energy) through phase-space filling, carrier-exciton scattering, Stark effect etc. Considering the negligible excited species at the direct exciton band in the presence of a lower lying indirect bandgap, the observed decay dynamics at the PB is not due to the relaxation and recombination

of excitons themselves, but instead due to the carriers at the indirect band edge. This is clearly seen in **Figure 3(c)**, where the PB decay dynamics of both films shows long lifetimes up to tens of ns, which is much longer than the typical values of excitons. The decay dynamics were fitted using the bi-exponential decay formula:

$$I(t) = A_1 \exp(-t/\tau_1) + A_2 \exp(-t/\tau_2)$$

where τ_1 and τ_2 are the short and long recombination lifetimes. Non single-exponential decay is commonly seen in many perovskite polycrystalline films, and usually arose from distributions of crystal size or trap states, non-radiative/radiative recombination and surface/bulk recombination difference, etc.[18] The summarized kinetic fit parameters of the decay lifetime are presented in Table S1. For the NSC thin-films, a fast component of $\tau_1 \approx 7$ ns and $\tau_1 \approx 12$ ns along with the slower components of $\tau_2 \approx 23$ ns and $\tau_2 \approx 83$ ns were observed for $AgBiI_4$ and Ag_2BiI_5 thin-films. With DHC, a marked improvement in slower component of the excited state carrier lifetime was observed with values of $\tau_2 \approx 75$ ns and 133 ns for $AgBiI_4$ and Ag_2BiI_5 thin-films respectively. Similar observations can be made from the optical absorption spectra of NSC and DHC thin-films. As shown in Figure 3(a), the slope of absorption edge of $AgBiI_4$/Ag_2BiI_5 thin-films fabricated via DHC method is steeper as compared to the thin-films fabricated via normal spin coating technique, which is due to reduction of structural disorder. Hence, the enhanced carrier lifetime and stronger absorption at the bandedge can be correlated with the improved grain size and passivation of trap states in the thin-films fabricated by the DHC technique. Both $AgBiI_4$ and Ag_2BiI_5 thin films displayed moderate carrier densities (4.21×10^{14} cm^{-3} and 3.91×10^{14} cm^{-3} respectively) and good carrier mobilities (1.74 ± 0.3 cm^2 $V^{-1}s^{-1}$ and 2.26 ± 0.3 cm^2 $V^{-1}s^{-1}$ respectively) with a p-type character as characterized by Hall measurements.

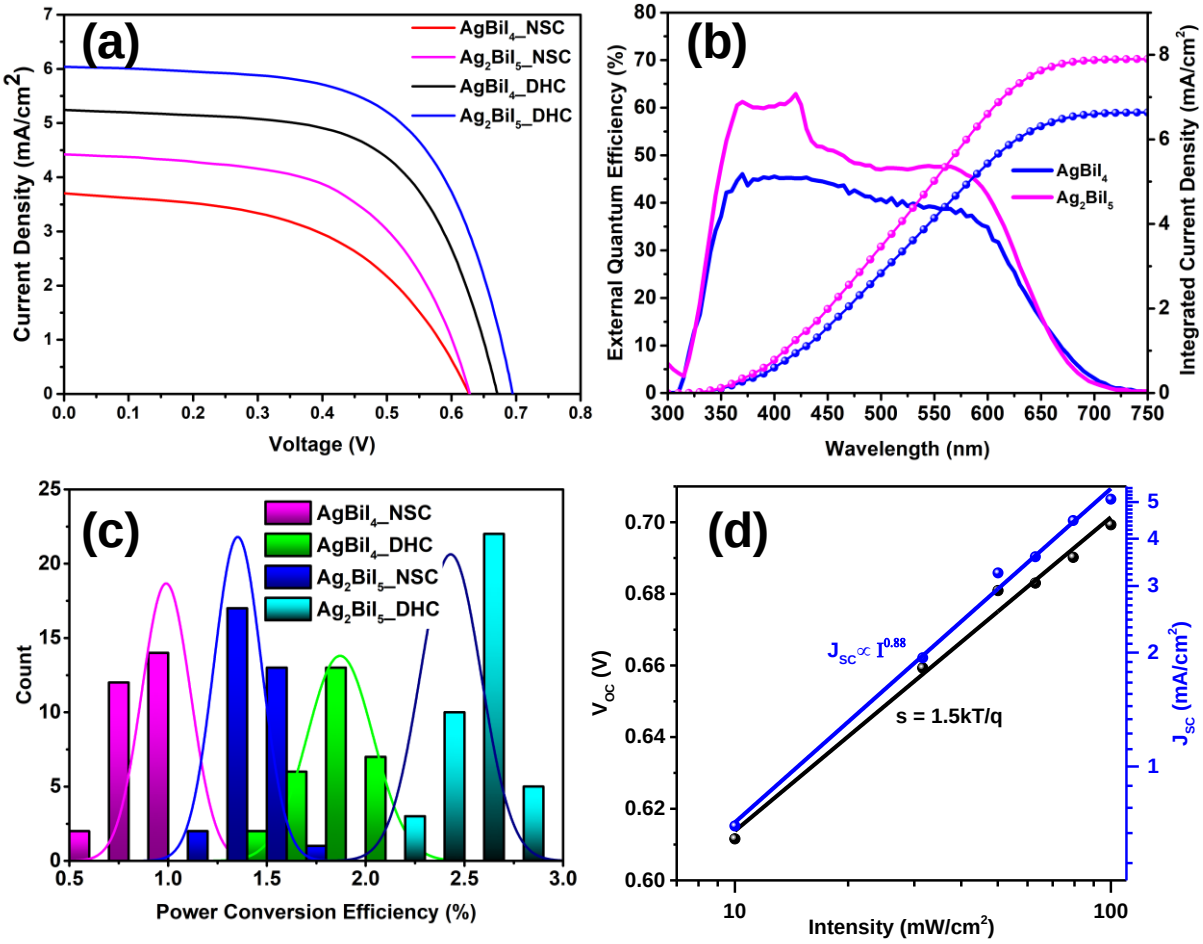

Figure 4: (a) current-voltage curves of best performing silver bismuth iodide-based solar cells, (b) Integrated current to photon conversion efficiency of dynamic hot casted silver bismuth iodide-based solar cell, (c) power conversion efficiency distribution of silver bismuth iodide based solar cell at different spin coating technique, (d) intensity dependent V_{OC} and J_{SC} evolution of dynamic hot casted Ag_2BiI_5-based solar cell

To further illustrate the effect on photovoltaic performance, we fabricated silver bismuth iodide-based mesoporous solar cells with a device configuration of FTO/c-TiO_2/m-TiO_2/absorber/(Poly[bis(4-phenyl)(2,4,6-trimethylphenyl)amine))(PTAA)/Au. The valence band maximum (VBM) was determined to be -5.5 eV and -5.7 eV for $AgBiI_4$ and Ag_2BiI_5 respectively using Ultraviolet Photoelectron Spectroscopy (UPS) measurement. Using optical bandgap values, the conduction band minimum was found to be -4.0 eV and -3.8 eV for $AgBiI_4$

and Ag_2BiI_5 respectively. To ensure efficient charge extraction, we used PTAA (without dopant) as hole transporting material (HTM) which offers favorable alignment (Figure S4). The current density-applied voltage (*J-V*) characteristics of the mesoporous solar cells are shown in **Figure 4(a)** and the best performing solar cell parameters are summarized in Table 1. Using the NSC technique, a current density (J_{SC}) of 3.7 mA cm^{-2}, open circuit voltage (V_{OC}) 0.63 V, fill factor (FF) of 51.4%, and a power conversion efficiency (PCE) of 1.2% was achieved with $AgBiI_4$-based solar cells. Whereas with Ag_2BiI_5 as an absorber material, the fabricated mesoscopic solar cell exhibited a current density of 4.42 mA cm^{-2}, open circuit voltage of 0.63 eV and FF of 57.6% which translates to a 1.6% PCE at 1 Sun illumination. The performance of these solar cells was comparable with the previous studies on similar compounds.[10, 11] However, it is worth noting here that the fabrication of these devices were conducted under ambient atmosphere with an average relative humidity of ≥ 65%, whereas earlier reports on silver bismuth iodides-based solar cells utilized inert-gas filled glovebox for fabrication. In comparison to the NSC method, solar cells fabricated by the dynamic hot casting technique exhibited marked improvement in PCEs with higher V_{OC}, J_{SC}, and FF. The champion devices yielded power conversion efficiencies of 2.18% and 2.62% under 1 Sun illumination, which is the highest to date for solution processed $AgBiI_4$ and Ag_2BiI_5-based solar cells. The large improvement in PCEs could be attributed to better surface coverage on mesoporous TiO_2 along with the reduction of trap states, resulting in improved excited-state carrier lifetime. Moreover, the solar cells also exhibited high degree of reproducibility in overall efficiencies (**Figure 4(c)**) and negligible hysteresis (**Figure S5**). **Figure 4(b)** illustrates the incident photon to current conversion efficiency (IPCE) over the spectral range of 300 to 750 nm for $AgBiI_4$ and Ag_2BiI_5-based solar cells fabricated by DHC. The IPCE spectra shows good agreement with the absorption onset of the thin-films. However, the integrated current densities from IPCE spectra were calculated to be 6.6 mA cm^{-2} and 7.9 mA cm^{-2} as compared to 4.42 mA cm^{-2} and 6.04 mA cm^{-2}, calculated from *J-V* measurement by under illumination by simulated AM1.5 sun for

$AgBiI_4$ and Ag_2BiI_5 respectively. This indicates better performance of the silver bismuth iodide based solar cells under low intensity light (maximum PCE of 3.3% at 31.6 mW cm^{-2}). To understand the mismatch between IPCE and solar spectrum current densities, *J-V* measurements of Ag_2BiI_5-based solar cells were performed under varying light intensities, ranging from 10 mW cm^{-2} to 100 mW cm^{-2}. **Figure 4(d)** illustrates the dependence of J_{SC} and V_{OC} on the solar spectrum intensity. The current generation depicted a sublinear relationship with gradually saturation at higher intensities, indicating a lower charge collection efficiency at higher light intensity. This can be attributed to an imbalanced electron-hole mobilities or space-charge limited photocurrent due to non-optimal thickness of electron/hole transporting layers.[19] A semi-logarithmic plot of V_{OC} against light intensity exhibited a slope of $1.5kT/q$, indicating a trap assisted recombination near V_{OC}. This was also confirmed by variation of the FF at different light intensities (Figure S7). A maximum FF of 68.6% is achieved at 31.6 mW cm^{-2} light intensity, implying minimal charge carrier recombination at relatively lower light intensity due to low carrier generation.[20] Figure S8 shows the atmospheric stability of silver bismuth iodide-based solar cells. Our devices were stored in an ambient atmosphere at 20 ℃ with a humidity of 60-75% and remained stable over a month. The V_{OC} of the devices remained nearly the same within this period, but the efficiencies dropped slightly due to a reduction in the current density, possible due to degradation at the hole transport material (HTM) interface.

Table1: *J-V* parameters of best performing solar cell devices.

Type of spin coating	Nominal composition	V_{OC} (V)	J_{SC} (mA cm^{-2})	FF (%)	PCE (%)
Normal spin coating	$AgBiI_4$	0.63	3.70	51.40	1.2
	Ag_2BiI_5	0.63	4.42	57.60	1.6

Dynamic Hot casting	$AgBiI_4$	0.67	5.24	62.09	2.2
	Ag_2BiI_5	0.69	6.04	62.40	2.6

In summary, we have introduced a modified technique of spin coating for lead-free bismuth-based ternary halide solar cells. In this dynamic hot casting technique, the preheated precursor solutions were drop casted onto preheated substrates during spinning in ambient atmosphere. With faster crystallization and rapid removal of precursor solution, micron-sized grains were observed; resulting in improved photovoltaic performance from silver bismuth iodide based mesoscopic solar cells. Interestingly, the solar cells performed better under lower intensity light that can further be explored for indoor applications. With further optimization in device fabrications, the power conversion efficiency can be improved.

Experimental Section

Materials and Methods:

BiI_3 and AgI (both are 99.999% pure and brought from Sigma-Aldrich) were used as received. For $AgBiI_4$, 0.5 mol AgI and 0.6 mol BiI_3 and for Ag_2BiI_5, 0.6 mol AgI and 0.3 mol BiI_3 were dissolved in 1 mL DMF: DMSO (1:1) mixture. Fluorine-doped tin oxide (FTO) coated glass slides were first patterned by chemical etching with Zn powder and HCl. After pattering, the glass slides were thoroughly cleaned using soap solution, DI water and ethanol. The compact TiO_2 layer was deposited by spay pyrolysis of 400 µL of titanium diisopropoxide bis(acetylacetonate) solution (75% in 2-propanol) and 600 µL of acetylacetone, diluted in 2-propanol (1:5 v/v). Mesoporous TiO_2 paste (GreatCell-30NRD) was diluted with ethanol (1:4 w/w) and spin coated onto FTO substrates and annealed at 500 ℃ for 15 minutes. The mesoporous substrates were plasma cleaned prior to spin coating precursor solution. Around 60

μL precursor solution was spread onto the substrate, following by spin coating at 7000 rpm for 30 s during normal spin coating method. Chlorobenzene was used as antisolvent after 20 s of spinning time. For dynamic hot casting, the substrates and the precursor solutions were preheated at 100 ℃ before spin coating. The substrates were subsequently annealed at 160 ℃ for 15 min on a hotplate. After deposition of the absorber layer, PTAA (10 mg mL^{-1} in Toluene) was spin-coated at 5000 rpm for 30 s. Subsequently, a 70 nm Au electrode was evaporated on top of the HTM layer. The device area was 0.2 cm^2 as defined by a metal shadow mask during *J-V* characterizations.

X-ray diffraction was carried out at room temperature using a Bruker D8 Advanced Diffractometer (Bragg-Brentano geometry) with Cu-Kα radiation (λ = 1.5418 Å). Field Emission Scanning Electron Microscope (JEOL, JSM-7600F, operated at 5 kV) was used for morphology and cross-section analysis of the photovoltaic devices. UV-Vis spectrophotometer (Shimadzu-3600) with integrated sphere attachment (ISR-3100) and 20 nm slit-width was used for absorption spectroscopy in the wavelength range of 300-800 nm. Transient absorption measurements were performed using an integrated Helios and EOS setup (Ultrafast Systems LLC) with 400 nm excitation pulses by doubling the output from the Coherent Legend system. The J-V curves of the devices were characterized using solar simulator (San-EI Electric, XEC 301S) at AM1.5 illumination (power density 1000 W m^{-2}). EQE/IPCE measurement was carried out by PV300 (Bentham) equipped with Xenon/quartz halogen monochromatic light source.

The UPS measurements were carried out using a VG ESCA Lab system. An integrated ultrahigh vacuum (UHV) system equipped with the fast-entry lock chamber and analysis chamber with typical base pressure in the range of ~10^{-10} mbar. To provide ultraviolet irradiation impinged to the sample, the analysis chamber is equipped with a He discharge lamp. The UV source was an unfiltered He I (21.2 eV) excitation and the sample was biased at -5V to extract the low-energy secondary cutoff. The UV light spot size on the sample is about 1 mm in diameter.

Supporting Information

Supporting Information is available from the Wiley Online Library or from the author.

Acknowledgements
This research was supported by the National Research Foundation, Prime Minister's Office, Singapore under its Competitive Research Programme (CRP Award No. NRF-CRP14-2014-03) and through the Singapore–Berkeley Research Initiative for Sustainable Energy (SinBeRISE) CREATE Program. T. C. S. would like to acknowledge the financial support from the Ministry of Education Academic Research Fund Tier 1 Grant RG173/16, and Tier 2 Grants MOE2015-T2-2-015 and MOE2016-T2-1-034. Arramel and A. T. S. W. would like to acknowledge the financial support from research grant from MOE Tier 3 program (MOE2014-T3-1-004).

Received: ((will be filled in by the editorial staff))
Revised: ((will be filled in by the editorial staff))
Published online: ((will be filled in by the editorial staff))

References

[1] (a) NREL Efficiency Chart (Acessed from https://www.nrel.gov/pv/assets/pdfs/pv-efficiencies-07-17-2018.pdf on 30/09/2018), (b) H. Zhang, J. Mao, H. He, D. Zhang, H. L. Zhu, F. Xie, K. S. Wong, M. Grätzel, W. C. H. Choy, Adv. Energy Mater. 2015, 5, 1501354..
[2] A. Abate, Joule 2017, 1, 659.
[3] A. Ciccioli, A. Latini, J. Phys. Chem. Lett. 2018.
[4] a) A. Mei, X. Li, L. Liu, Z. Ku, T. Liu, Y. Rong, M. Xu, M. Hu, J. Chen, Y. Yang, M. Grätzel, H. Han, Science 2014, 345, 295; b) T. Leijtens, G. E. Eperon, N. K. Noel, S. N. Habisreutinger, A. Petrozza, H. J. Snaith, Adv. Energy Mater. 2015, 5, 1500963; c) Z. Hong, C. Jiaqi, L. Dan, L. Francis, M. Jian, L. Chunjun, J. A. K.-Y., G. Michael, C. W. C. H., Adv. Mater. 2017, 29, 1604695; d) H. Zhang, X. Ren, X. Chen, J. Mao, J. Cheng, Y. Zhao, Y. Liu, J. Milic, W.-J. Yin, M. Grätzel, W. C. H. Choy, Energy Environ. Sci. 2018, 11, 2253.
[5] a) T. Krishnamoorthy, H. Ding, C. Yan, W. L. Leong, T. Baikie, Z. Zhang, M. Sherburne, S. Li, M. Asta, N. Mathews, S. G. Mhaisalkar, J. Mater. Chem. A 2015, 3, 23829; b) F. Hao, C. C. Stoumpos, D. H. Cao, R. P. H. Chang, M. G. Kanatzidis, Nat. Photonics 2014, 8, 489; c) M. H. Kumar, S. Dharani, W. L. Leong, P. P. Boix, R. R. Prabhakar, T. Baikie, C. Shi, H. Ding, R. Ramesh, M. Asta, M. Graetzel, S. G. Mhaisalkar, N. Mathews, Adv. Mater. 2014, 26, 7122.
[6] S. Shao, J. Liu, G. Portale, H. H. Fang, G. R. Blake, G. H. t. Brink, L. J. A. Koster, M. A. Loi, Adv. Energy Mater. 2018, 8, 1702019.
[7] a) P. C. Harikesh, H. K. Mulmudi, B. Ghosh, T. W. Goh, Y. T. Teng, K. Thirumal, M. Lockrey, K. Weber, T. M. Koh, S. Li, S. Mhaisalkar, N. Mathews, Chem. Mater. 2016, 28, 7496; b) H. Robert, B. Riley, O. Anna, S. Vladan, S. Samuel, W. Mark, K. Hyunho, A. Austin, P. John, K. Rachel, P. Jeremy, W. Evelyn, B. Moungi, B. Vladimir, B. Tonio, Chem. Eur. J. 2016, 22, 2605; c) M. Lyu, J.-H. Yun, M. Cai, Y. Jiao, P. V. Bernhardt, M. Zhang, Q. Wang, A. Du, H. Wang, G. Liu, L. Wang, Nano Res. 2016, 9, 692; d) B.-W. Park, B. Philippe, X. Zhang, H. Rensmo, G. Boschloo, E. M. J. Johansson, Adv. Mater. 2015, 27, 6806.
[8] a) B. Ghosh, S. Chakraborty, H. Wei, C. Guet, S. Li, S. Mhaisalkar, N. Mathews, J. Phys. Chem. C 2017, 121, 17062; b) B. Ghosh, B. Wu, H. K. Mulmudi, C. Guet, K. Weber, T. C. Sum, S. G. Mhaisalkar, N. Mathews, ACS Appl. Mater. Interfaces 2018.
[9] T. Oldag, T. Aussieker, H. Keller, C. Preitschaft, A. Pfitzner, Z. Anorg. Allg. Chem 2005, 631, 677.

[10] Y. Kim, Z. Yang, A. Jain, O. Voznyy, G.-H. Kim, M. Liu, L. N. Quan, F. P. García de Arquer, R. Comin, J. Z. Fan, E. H. Sargent, Angew. Chem. 2016, 128, 9738.
[11] H. Zhu, M. Pan, M. B. Johansson, E. M. J. Johansson, ChemSusChem 2017, 10, 2592.
[12] I. Turkevych, S. Kazaoui, E. Ito, T. Urano, K. Yamada, H. Tomiyasu, H. Yamagishi, M. Kondo, S. Aramaki ChemSusChem 2017, 10, 3754.
[13] L. F. Mashadieva, Z. S. Aliev, A. V. Shevelkov, M. B. Babanly, J. Alloys Compd. 2013, 551, 512.
[14] Z. Xiao, W. Meng, D. B. Mitzi, Y. Yan, J. Phys. Chem. Lett. 2016, 7, 3903.
[15] K. W. Jung, M. R. Sohn, H. M. Lee, I. S. Yang, S. D. Sung, J. Kim, E. Wei-Guang Diau, W. I. Lee, Sustainable Energy & Fuels 2018, 2, 294.
[16] S. S. Shin, J. P. Correa Baena, R. C. Kurchin, A. Polizzotti, J. J. Yoo, S. Wieghold, M. G. Bawendi, T. Buonassisi, Chem. Mater. 2018, 30, 336.
[17] a) X. Manda, H. Fuzhi, H. Wenchao, D. Yasmina, Z. Ye, E. Joanne, G. W. Angus, B. Udo, C. Yi‐Bing, S. Leone, Angew. Chem. Int. Ed. 2014, 53, 9898; b) N. J. Jeon, J. H. Noh, Y. C. Kim, W. S. Yang, S. Ryu, S. I. Seok, Nat. Mater. 2014, 13, 897.
[18] a) V. D'Innocenzo, A. R. Srimath Kandada, M. De Bastiani, M. Gandini, A. Petrozza, J, Am. Chem. Soc. 2014, 136, 17730; b) A. D. Wright, R. L. Milot, G. E. Eperon, H. J. Snaith, M. B. Johnston, L. M. Herz, Adv. Funct. Mater. 2017, 27, 1700860; c) W. Bo, N. H. Tiep, K. Zhiliang, H. Guifang, G. David, M. Nripan, F. H. Jin, S. T. Chien, Adv. Energy Mater. 2016, 6, 1600551; d) S. J. Kim, J. Byun, T. Jeon, H. M. Jin, H. R. Hong, S. O. Kim, ACS Appl. Mater. Interfaces 2018, 10, 2490.
[19] V. D. Mihailetchi, J. Wildeman, P. W. M. Blom, Phys. Rev. Lett. 2005, 94, 126602.
[20] D. Zhao, W. Ke, C. R. Grice, A. J. Cimaroli, X. Tan, M. Yang, R. W. Collins, H. Zhang, K. Zhu, Y. Yan, Nano Energy 2016, 19, 88.

A dynamic hot casting technique is presented to fabricate silver bismuth iodide-based perovskite solar cells under ambient atmosphere with power conversion efficiencies above 2.5%. The enhanced solar cell performance can be ascribed to pin-hole free thin-film formation with uniform morphology, micron-sized crystalline grains, and long carrier lifetime.

Keyword: perovskite solar cells, lead-free perovskites, Bi-based ternary halides, dynamic hot casting

*Biplab Ghosh, Bo Wu, Guo Xintong, Padinhare C. Harikesh, Rohit Abraham John, Tom Baikie, Arramel, Andrew T. S. Wee, Claude Guet, Tze Chien Sum, Subodh Mhaisalkar, and Nripan Mathews**

Superior performance of Silver Bismuth Iodide photovoltaics fabricated via dynamic hot-casting method under ambient condition

ToC figure ((Please choose one size: 55 mm broad × 50 mm high **or** 110 mm broad × 20 mm high. Please do not use any other dimensions))